Showcasing research from the Laboratory of Dr Yanan Yue at the School of Power and Mechanical Engineering, Wuhan University, China.

Title: Molecular dynamics study of interfacial thermal transport between silicene and substrates

This paper reports a study of energy coupling between silicene and different substrate materials by using a transient heating molecular dynamics method. Important findings include the interfacial heat conductance can be greatly improved with increasing temperature from 100 K to 400 K and with increasing interfacial coupling strength. It is also found amorphous structure of substrate could facilitate the interfacial thermal transport between this atomic layer material and substrate. The work is performed by collaborators from University of Nebraska-Lincoln in USA, Shanghai Jiao Tong University and Wuhan University in China.

As featured in:

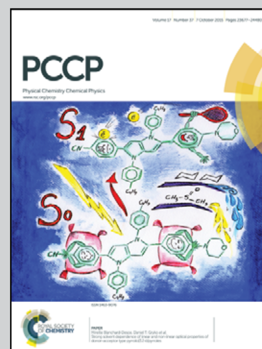

See Zhihuai Xiao, Yanan Yue *et al.*, *Phys. Chem. Chem. Phys.*, 2015, **17**, 23704.

www.rsc.org/pccp

Registered charity number: 207890

PCCP

COMMUNICATION

Cite this: *Phys. Chem. Chem. Phys.*, 2015, **17**, 23704

Received 8th June 2015, Accepted 31st July 2015

DOI: 10.1039/c5cp03323c

www.rsc.org/pccp

Molecular dynamics study of interfacial thermal transport between silicene and substrates

Jingchao Zhang,[a] Yang Hong,[b] Zhen Tong,[c] Zhihuai Xiao,*[d] Hua Bao[c] and Yanan Yue*[d]

In this work, the interfacial thermal transport across silicene and various substrates, *i.e.*, crystalline silicon (c-Si), amorphous silicon (a-Si), crystalline silica (c-SiO_2) and amorphous silica (a-SiO_2) are explored by classical molecular dynamics (MD) simulations. A transient pulsed heating technique is applied in this work to characterize the interfacial thermal resistance in all hybrid systems. It is reported that the interfacial thermal resistances between silicene and all substrates decrease nearly 40% with temperature from 100 K to 400 K, which is due to the enhanced phonon couplings from the anharmonicity effect. Analysis of phonon power spectra of all systems is performed to interpret simulation results. Contradictory to the traditional thought that amorphous structures tend to have poor thermal transport capabilities due to the disordered atomic configurations, it is calculated that amorphous silicon and silica substrates facilitate the interfacial thermal transport compared with their crystalline structures. Besides, the coupling effect from substrates can improve the interface thermal transport up to 43.5% for coupling strengths χ from 1.0 to 2.0. Our results provide fundamental knowledge and rational guidelines for the design and development of the next-generation silicene-based nanoelectronics and thermal interface materials.

Silicene, analogous to graphene, is a two-dimensional (2D) monolayer of silicon atoms constructed in hexagonal lattices with a slight local buckling.[1] It has attracted great attention due to its exceptionally high crystallinity and unusual electronic properties.[2–4] In contrast to the high thermal conductivity (κ) of graphene, the in-plane thermal conductivity of silicene is reported to be around 20–60 W m^{-1} K^{-1}, which is much lower than that of crystalline silicon ($\sim$140 W m^{-1} K^{-1} at room temperature).[5–7] The high electric transport capability and low thermal conductivity of silicene make it a promising thermoelectric material for next generation nano-devices and offer new insights for low-dimensional materials and related applications.

Phonon thermal transport in the lateral directions of silicene nanoribbons (SNRs) has been investigated by various numerical studies. Using the NEMD method, Zhou *et al.*[8] calculated the κ value of SNRs to be 61.7 and 68.5 W m^{-1} K^{-1}, respectively, for armchair and zigzag boundaries. Yang *et al.*[9] predicted the phonon lattice conductivity of silicene to be around 26 W m^{-1} K^{-1} using first principles calculations, which is much lower than that of bulk silicon ($\sim$140 W m^{-1} K^{-1}). Also using first-principles calculation with single mode relaxation time approximation, Xie *et al.*[10] predicted a lower thermal conductivity of silicene (to be around 10 W m^{-1} K^{-1}). A thermal conductivity value of 5.5 W m^{-1} K^{-1} is calculated using the equilibrium molecular dynamics (EMD) approach for all sizes considered.[11] Due to the special buckling structure in silicene, it is reported that its in-plane thermal conductivity can be tuned by applying appropriate tensile strains to distort the hexagonal lattice structures.[7]

Despite the fact that in-plane phonon thermal transport in silicene has been studied extensively, the interfacial thermal transport across silicene and substrate materials remains intact. To address this issue, thermal transport across silicene and multiple substrates (c-Si, a-Si, c-SiO_2, a-SiO_2) is calculated in this work. A fast transient technique is applied to characterize the thermal contact resistance (R) in the hybrid structures. Effects of temperature, substrate crystallinity and interfacial coupling strength are discussed to comprehensively understand the interface thermal transport across the atomic silicene structure and substrates. Analysis of phonon power spectra of the hybrid silicene substrate systems is performed to interpret the calculated results.

In recent studies of silicene, quite a few empirical potentials have been proposed to describe the Si–Si interactions in silicene. Tersoff potential[12] has been widely used to describe the Si atom interactions in bulk silicon and silicon nanotubes. Wang *et al.*,[13] Li *et al.*[5] and Hu *et al.*[2] employed the Tersoff potential to investigate the thermal conductivity of free-standing and

[a] *Holland Computing Center, University of Nebraska-Lincoln, Lincoln, NE 68588, USA*
[b] *Department of Chemistry, University of Nebraska-Lincoln, Lincoln, NE 68588, USA*
[c] *University of Michigan-Shanghai Jiao Tong University Joint Institute, Shanghai Jiao Tong University, Shanghai 200240, China*
[d] *School of Power and Mechanical Engineering, Wuhan University, Wuhan, Hubei 430072, China. E-mail: xiaozhihuai@126.com, yyue@whu.edu.cn*

This journal is © the Owner Societies 2015

supported single layer silicene. The calculated bond length and thermal conductivities of silicene are in good agreement with the predictions from first principles calculation.[14–16] While on the other hand, due to the Tersoff potential employed, the buckled structure of silicene was not captured and the system has a planar equilibrium structure. The modified Tersoff potential by Kumagai *et al.*[17] preserved the forms of Tersoff potential functions and soundly reproduced the elastic constants of diamond silicon as well as the cohesive energies and equilibrium bond lengths of silicon polytypes. The proposed angular-dependent term is critical to give an improved description of the melting point. In this work, this modified Tersoff potential is found to be able to maintain the buckled structure in free standing silicene with a buckling distance of 0.64 Å. Considering its inheritance from the Tersoff potential and the improved features, the authors employed it to describe the Si–Si interactions in monolayer silicene. In other studies, Pei *et al.*[7] used the MEAM potential[18] to explore the dependence of thermal conductivity of silicene on tensile stain and isotopic doping. Liu *et al.*[19] calculated the thermal conductivity using both Tersoff and Stillinger–Weber (SW) potentials.[20] Using a modified SW potential, Zhang *et al.*[11] characterized the thermal conductivity of silicene using non-equilibrium molecular dynamics. Some discrepancies exist among the calculated thermal conductivities with different potentials, but the calculated results are all on the same magnitude.

MD calculations in the work are performed by using the large-scale atomic/molecular massively parallel simulator (LAMMPS).[21] The interactions between Si–Si, Si–O atoms in silicene and c-Si, a-Si, c-SiO_2 and a-SiO_2 substrates are described by the Tersoff potentials.[17,22] Couplings between silicene and substrates are modeled by Lennard-Jones (LJ) potential $V(r) = 4\chi\varepsilon[(\sigma/r)^{12} - (\sigma/r)^6]$, where ε and σ are the energy and distance parameters with units eV and Å, respectively; χ represents the coupling strength between the substrate material and the supported silicene. The ε and σ values are calculated from the universal force field (UFF),[23] where ε_{Si-Si} = 0.0174398 eV, σ_{Si-Si} = 3.8264 Å, ε_{Si-O} = 0.0067376 eV and σ_{Si-O} = 3.4542 Å. Cutoff distance r_c is equal to $3.5\sigma_{Si-Si}$ for Si–Si interactions and $3.5\sigma_{Si-O}$ for Si–O interactions. Atomic configurations of the hybrid systems are shown in Fig. 1(a)–(d). The distance between silicene and substrates is set as 4.295 Å. An initial buckling distance of 0.85 Å is used in the silicene structures, which is proved to be the stable distance in previous MD study,[7] and within the range of 0.44–1 Å from *ab initio* calculations.[14,24,25] Periodic boundary conditions are applied to the lateral (x and y) directions of both silicene and the substrates. Free boundary conditions are used in the out-of-plane (z) direction. To remain consistent, the same silicene with dimensions of 105.374 × 95.4 ($x \times y$) $Å^2$ are used in all hybrid structures. A slight lattice mismatch of 1.74% and 3.68% is induced to the c-Si and c-SiO_2 substrates to fit the lattice parameter of silicene. Dimensions of c-Si, a-Si, c-SiO_2 and a-SiO_2 are equal to 105.374 × 94.704 × 85.386 $Å^3$ ($x \times y \times z$), 105.374 × 95.4 × 89.997 $Å^3$ ($x \times y \times z$), 105.231 × 95.662 × 87.002 $Å^3$ ($x \times y \times z$) and 105.374 × 95.4 × 89.663 $Å^3$ ($x \times y \times z$) respectively. A time step of 0.5 fs (1 fs = 10^{-15} s) is used for all calculations.

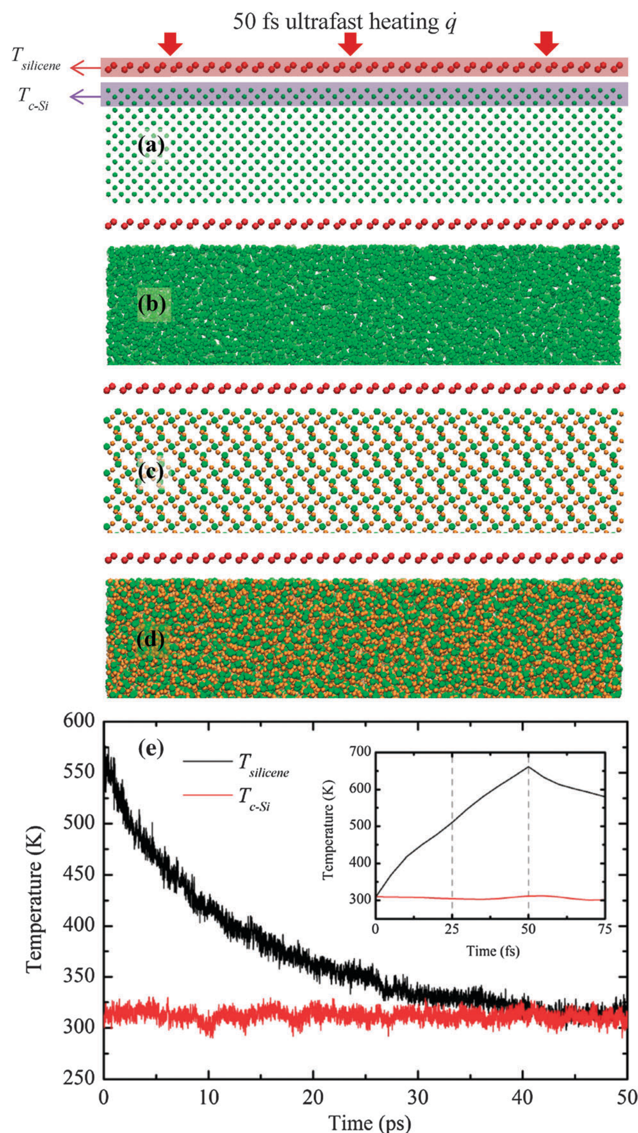

Fig. 1 (a–d) Atomic configurations of silicene/c-Si, silicene/a-Si, silicene/c-SiO_2 and silicene/a-SiO_2 hybrid systems. Periodic boundaries are applied in the lateral (x and y) directions. Free boundary conditions are used in the out-of-plane (z) direction. (e) Illustration of the transient heating technique for the silicene/c-Si system. The first 75 fs heating process is depicted in the inset.

NEMD simulations are widely used to calculate the thermal contact resistance (R) at the interfaces of bulk heterostructures. After the hybrid system reaches the equilibrium state, two groups of atoms are selected to add/subtract thermal energies respectively. After a steady temperature gradient is established, the interfacial thermal resistance can be calculated using the equation

$$R = \frac{\Delta T \cdot A}{q}, \qquad (1)$$

where ΔT is the temperature bias, A is the cross-section area, and q is the heat flux along the heat conduction direction. Using this approach, R between SiC and graphite is calculated to be ~(1–7) × 10^{-10} K m^2 W^{-1}.[26] Subbarayan *et al.*[27] calculated

R between Si and SiO_2 to be (0.503–0.518) $\times 10^{-9}$ K m^2 W^{-1}. For 2D materials like graphene and silicene, the thermal resistance in the lateral direction can also be calculated by the NEMD method. Zhang *et al.*[28] characterized the Kapitza resistance in the bending areas of graphene to be 1.48×10^{-11} K m^2 W^{-1} at temperature 300 K. The thermal contact resistance at the graphene-silicene monolayer is calculated to be $\sim 4 \times 10^{-9}$ K m^2 W^{-1}.[29] In traditional NEMD simulations, when a heat flux is constantly imposed on a group of atoms, the local temperatures in the heating/cooling areas are altered by variations of the atomic velocities. The energy exchange in/near the heated areas is very fast and kinetic and potential energies are unbalanced. Therefore, the temperatures recorded near the heat baths could be illusory. In hybrid bulk systems, the heat baths are normally far from the hetero interfaces. After the temperature gradient reaches the steady state in NEMD calculations, the temperature bias (ΔT) across the interface will be recorded and used to calculate the thermal resistance. Temperature points adjacent to the interfaces from both sides are used to characterize the temperature difference. This is a popular approach for R calculations which has been successfully applied in various systems.[30–34] While for membrane systems like silicene, the NEMD method for R characterization might not be applicable since the heat baths will be directly applied to the monolayer atomic structure. For this reason, the transient pulse heating approach is applied in this work.

A similar method has been applied to calculate interfacial thermal resistance at various 2D interfaces such as silicene/graphene,[35] boron-nitride/graphene,[36] MoS_2/graphene,[37] graphene/silicon[38] and graphene/copper.[39] For example, in the silicene/c-Si hybrid system, after 300 ps (1 ps = 10^{-12} s) canonical ensemble (*NVT*) calculations, the system reaches the steady state at 300 K. Consecutively, another 200 ps microcanonical ensemble (*NVE*) calculations are performed to allow the system to be fully relaxed. Then a 50 fs (1 fs = 10^{-15} s) ultrafast thermal impulse is applied to the supported silicene, as shown in Fig. 1(a). After the heat impulse, temperature of the silicene (T_{silicene}) reaches $\sim$650 K while temperature of the c-Si ($T_{\text{c-Si}}$) substrate remains unchanged, as illustrated in the inset of Fig. 1(e). In the following thermal relaxation process, interfacial thermal transport from silicene to substrates is the only channel for the thermal energy dissipations in silicene. Temperatures of the supported silicene, top three layers of Si, and total energies of silicene (E_t) are recorded each time step for post-processing. The outputs are averaged every 100 time steps to suppress data noise. In order to obtain smooth temperature evolutions during thermal relaxation, a temperature difference $\Delta T(T_{\text{silicene}} - T_{\text{c-Si}}) >$ 300 K is found to be necessary. Temperatures of silicene and top layers of c-Si in the 50 ps thermal relaxation process are shown in Fig. 1(e). Given the temperature and energy evolutions of the silicene system, R between silicene/Si can be calculated using the equation

$$\partial E_t/\partial t = A\cdot(T_{\text{silicene}} - T_{\text{c-Si}})/R, \qquad (2)$$

where E_t is the system energy of the supported silicene and A is the surface area. An instant R value can be calculated at each time step according to the local energy changing rate and the corresponding temperature difference. We have tried this method and found that it was subject to the noise in the energy decay and the calculated interface thermal resistance has very large uncertainty. As the energy decay is driven by the temperature difference $\Delta T = T_{\text{silicene}} - T_{\text{c-Si}}$, the silicene energy changes against $\int \Delta T \mathrm{d}t$ can be plotted and it is observed that the E_t profile has a linear relationship with $\int \Delta T \mathrm{d}t$. Each segment can represent the interfacial thermal transport efficiency at certain temperature levels, and it can be concluded that the thermal transport is very steady during the transient process and the overall fitting method can be used. Therefore, it is speculated that the overall system temperature has much larger effects than the transient temperature on interfacial thermal transport. If R has little variation within the temperature range during thermal relaxation, a constant R value can be substituted into eqn (2) to predict the E_t profile. In such a scenario, the interfacial thermal resistance can be calculated by best fitting of the E_t profile using the least squares method (LSM).

Take the silicene/c-Si hybrid system as an example, after the system reaches thermal equilibrium and is fully relaxed at temperature 300 K, a thermal impulse $\dot{q} = 3.16 \times 10^{-4}$ W is imposed on the supported silicene for 50 fs. In the following 50 ps thermal relaxation, the energy decay profile of silicene is recorded and fitted using the integral form of eqn (2),

$$E_t = E_0 + (A/R)\cdot\int_0^t (T_{\text{silicene}} - T_{\text{c-Si}})\mathrm{d}t, \qquad (3)$$

where E_0 is the initial energy of the fitting process; T_{silicene} and $T_{\text{c-Si}}$ are illustrated in Fig. 1(e). The total energy (E_t) fitting results are shown in Fig. 2(a). It can be observed that the fitting curve soundly matches the calculated MD results, indicating the validity of eqn (2) to describe this physical process. The averaged R value resulting from five independent simulations is equal to 1.888×10^{-8} K m^2 W^{-1} with a standard deviation of 0.072, which is slightly lower than that between graphene and c-Si (3.52×10^{-8} K m^2 W^{-1}) at 300 K.[38] At the beginning stage of the fitting process, there is a small mismatch between the fitting curve and the calculated E_t results. This is due to the fact that after the 50 fs ultrafast heating process, kinetic and potential energies in silicene are in the non-equilibrium state and the calculated MD temperatures are inaccurate. The observed fitting mismatch at the early state will not affect the overall fitting result since it only lasts for several picoseconds. Energy fitting results for silicene on a-Si, c-SiO_2 and a-SiO_2 are shown in Fig. 2(b)–(d).

In practical applications, silicene-based devices are often placed under various working conditions at different temperatures. Thus it is of great interest to investigate temperature's effect on interfacial thermal transport. The initial temperatures of the MD systems are adjusted to 100 K, 150 K, 200 K, 250 K, 350 K and 400 K for thermal contact resistance characterization. To keep consistent with previous calculations, a 50 fs heat impulse with $\dot{q} = 3.16 \times 10^{-4}$ W is used in all transient heating processes. Calculated R results are shown in Fig. 3. For each data point, five independent simulations are performed to gain the averaged results and standard deviations. It is concluded from the results that the interfacial thermal resistance between

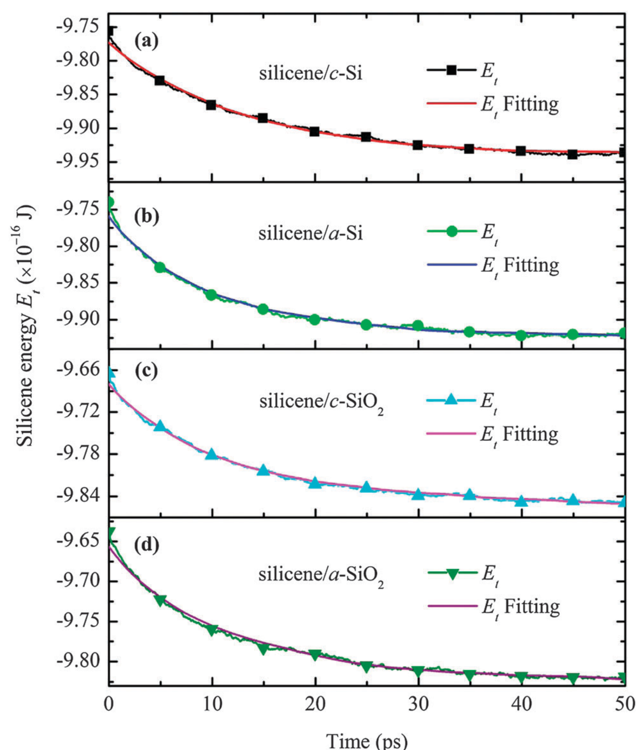

Fig. 2 (a–d) Energy fitting results of supported silicene for different hybrid systems at temperature 300 K. MD energy outputs are represented by dotted line profiles. Solid lines represent the fitting curves.

silicene and Si/SiO_2 substrates decreases monotonically with temperature. Maximum R decreases of 28.7%, 28.4%, 36.9% and 31.4% are calculated for c-Si, a-Si, c-SiO_2 and a-SiO_2 substrates respectively. This temperature dependence of R is in good agreement with previous calculations between silicene/graphene, graphene/copper and carbon nanotube (CNT)/SiO_2.[40–42] To better explain temperature's effect on thermal resistance, phonon density of state (PDOS) of silicene supported on a-Si and a-SiO_2 at temperatures 100 K and 400 K is analyzed. The PDOS can be calculated by taking the Fourier transform of the velocity autocorrelation function (VACF)

$$F(\omega) = 1/\sqrt{2\pi}\int_{-\infty}^{\infty} \mathrm{d}t\, e^{i\omega t} Z(t), \tag{4}$$

where $Z(t) = \langle \nu(0)\cdot\nu(t)\rangle / \langle \nu(0)\cdot\nu(0)\rangle$. Higher values of PDOS for a phonon with frequency ω means more states are occupied by it. And zero PDOS means no phonon with frequency ω exists in the system. The phonon power spectrum analysis provides a quantitative means to assess the power carried by phonons in a system. It is observed in Fig. 4(a) that at a temperature of 100 K, the phonon PDOS of silicene and silicon is mainly distributed in the region of 0–20 THz, which is the same as that reported in previous studies.[42–44] Since the phonon frequency does not depend on the amplitude of the oscillations, the PDOS of harmonic systems should be temperature-independent. However, when the temperature increases to 400 K, it is observed that both the PDOS of silicene and a-Si become broader, which indicates that the umklapp scattering mechanism is dominant

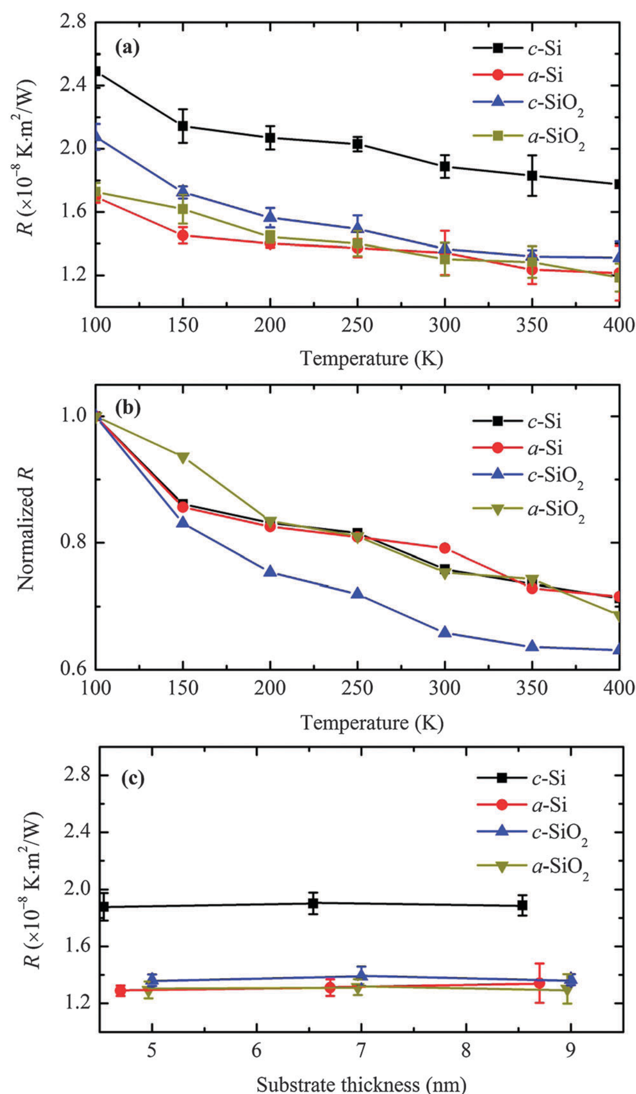

Fig. 3 (a) Dependence of interfacial thermal resistance (R) on temperature. Five independent simulations are performed in each case. The averaged results and standard deviations are represented by solid dots and error bars respectively. (b) Normalized R values with temperature. It can be observed that the c-Si, a-Si and a-SiO_2 substrates have similar effects on interfacial thermal resistance from 100 K to 400 K, while the silicene/c-SiO_2 heterostructure has a faster R drop within the same temperature range. (c) Substrate thickness effects on R. When the thickness decreases to $\sim$5 nm and $\sim$7 nm, the calculated R results do not have substantial changes, indicating size-independent R values in the out-of-plane z direction.

at this temperature range and the phonon anharmonicity is significant. The umklapp processes reduce the phonon mean free paths (MFP) on both sides of the interface and altered the PDOS distribution with more activated higher frequency phonons. Contributions from the high frequency phonons to thermal transport reduce the thermal contact resistance. Moreover, the three phonon scatterings become more furious at high temperatures, which will decompose the high frequency phonons into lower frequency branches and couple with the other phonons in the hybrid system, and as a result decrease the value of R.

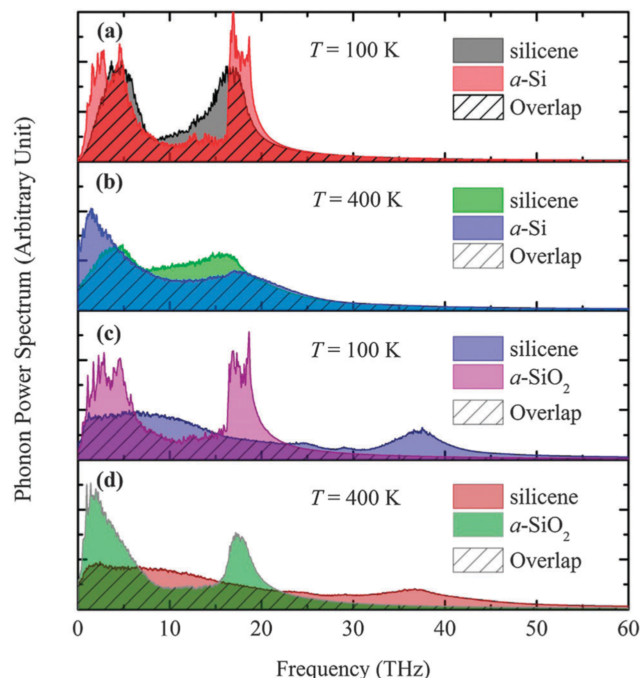

Fig. 4 (a and b) Phonon power spectra of silicene and top layers of a-Si at temperatures 100 K and 400 K. (c and d) Phonon power spectra of silicene and top layers of a-SiO_2 at temperatures 100 K and 400 K. It can be observed that as the temperature increases, the PDOS of both silicene and substrates is broadened. Meanwhile, the overlap area δ becomes larger with temperature, indicating better phonon transmissions across the interfaces. The calculated δ values are displayed in Table 1.

One of the crucial factors in determining the interfacial thermal resistance is the overlap of phonon states. To help compare the differences between the calculated results, the PDOS distributions are normalized with an integration area of 1 for each PDOS profile. If the phonon population with a certain ω value is low or zero, the energy propagation by phonons of that wave vector will be highly restricted. Therefore, the overlap areas between the PDOS with temperature need to be explored. To quantify this variation, an arbitrary unit variable, which is defined as $\delta = \int \omega A(\omega) d\omega$, is introduced to help assist the analyses.[45] $A(\omega)$ represents the intersection area at frequency ω. The area integration is proportional to the amount of energy transported across the interface by phonons at these frequency intervals. The calculated δ is equal to 0.81278 for silicene/a-Si at temperature 100 K and 0.86695 at temperature 400 K. Similar conclusions can be achieved from Fig. 4(c) and (d) for silicene/a-SiO_2. The PDOS overlap areas are calculated to be 0.65979 and 0.68662 at temperatures 100 K and 400 K separately. The calculated results are summarized in Table 1. Much attention should be paid to the fact that the size effect of silicene could be important in our silicene–substrate systems and thus affect our calculation on the temperature dependence of interfacial thermal transport. To address this concern, different thickness values of 50 and 70 Å (for silicene) are applied in calculations and the results are shown in Fig. 3(c). It is found that no obvious variation in interfacial thermal resistance is observed. Therefore, it can be regarded that the calculated interfacial thermal resistance for the domain in this work is not size-dependent.

Table 1 Comparison of the transmitted phonon energy through the interface: the integration of the overlap area multiplied by the corresponding frequency in PDOS of the interface materials

$\delta = \int \omega A(\omega) d\omega$	100 K	400 K
a-Si	0.81278	0.86695
a-SiO_2	0.65979	0.68662

Aside from the decreasing trend of R with temperature, another important discovery in this work is that the interfacial thermal resistances at amorphous interfaces are much lower than those at crystalline interfaces, as shown in Fig. 3. This phenomenon has also been reported in previous studies between graphene and SiC substrates.[45] This new discovery is contradictory to the traditional thought that amorphous structures always have worse thermal performance than crystalline structures. It is reported that the thermal conductivity of a-Si is only about one-hundredth of that of c-Si.[46] While when it comes to interfacial thermal transport in the cross-plane direction, the amorphous structures can facilitate the thermal transport across interfaces. The disordered atomic structure greatly enhances the phonon scatterings in the amorphous system. The shortened phonon mean free path and phonon relaxation time will give rise to decreased in-plane thermal conductivities. Meanwhile, it decomposes the high frequency phonons into multiple low frequency branches and couples with other phonons, which directly contribute to interfacial thermal transport.

Similar to those peculiar thermal properties of graphene,[47–49] in a recent study by Hu *et al.*,[50] a counter-intuitive phenomenon, in which the in-plane thermal conductivity (κ) of supported silicene can be either enhanced or suppressed by changing the surface crystal plane of the substrate, has been observed. By increasing the interfacial coupling strength (χ) in the 12-6 LJ potential, it is calculated that κ of silicene increases on 6H–SiC substrates and decreases on 3H–SiC substrates. This bilateral substrate effect is fundamentally different from that of previous graphene studies, which proved that substrates will always have negative effects on phonon transport in lateral directions.[51–53] In spite of this new discovery on the in-plane thermal transport of supported silicene, the coupling strength's effect on the out-of-plane thermal transport has not yet been studied. In this work, dependence of interfacial thermal resistance on coupling strength (χ) is calculated for c-Si, a-Si, c-SiO_2 and a-SiO_2 substrates. The initial temperature for all hybrid systems is set as 300 K. Different coupling strengths of χ = 1.0, 1.5 and 2.0 are applied. The calculated results are shown in Fig. 5. It is observed that the thermal contact resistance decreases monotonically with χ, indicating no bilateral effects for the substrates used in this work. The maximum decrease of R is calculated to be 35.9%, 43.5%, 29.4% and 38.1% for silicene/c-Si, silicene/a-Si, silicene/c-SiO_2 and silicene/a-SiO_2 respectively. The stronger coupling strength enhanced the phonon couplings at the interface, which directly contributes to the interfacial thermal transport and reduces the calculated R results.

In this work, interfacial thermal transport across silicene and various crystalline and amorphous substrates is studied

 This journal is © the Owner Societies 2015

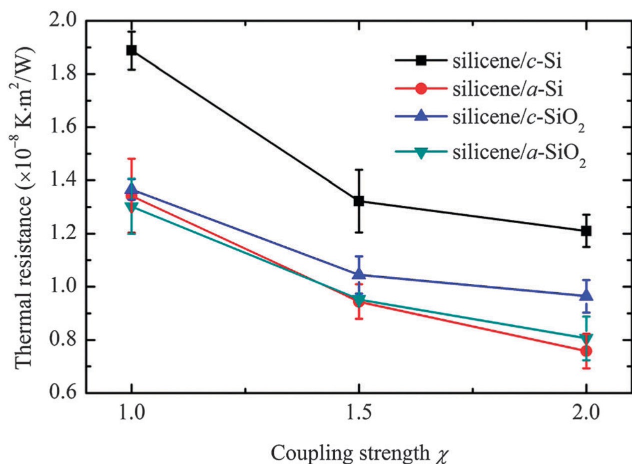

Fig. 5 Interfacial thermal resistance variations with LJ coupling strength χ.

using classical MD simulations. A fast transient technique is applied to calculate the interfacial thermal resistance. Compared to the traditional NEMD method, this technique can characterize the resistance within only 50 ps with higher accuracy. Effects of temperature, substrate crystallinity, and coupling strength on cross-plane thermal transport are discussed. It is found that the interfacial thermal resistance decreases monotonically with temperature. And contradictory to the traditional thought that amorphous structures always have negative effects on phonon thermal transport, it is calculated that amorphous silicon and silica can facilitate the interfacial thermal transport compared to their crystalline structures. The greater phonon scattering is the major factor that contributes to this peculiar phenomenon. Unlike the bilateral substrate effects reported on the in-plane thermal transport of silicene, the interfacial thermal resistances across silicene and c-Si, a-Si, c-SiO_2 and a-SiO_2 substrates have the same decreasing trend with enlarged coupling strength, which is the same as reported in previous studies of graphene structures.

Acknowledgements

J. Z. is grateful for the support from the UNL Holland Computing Center. Z. X. acknowledges the support from the National Natural Science Foundation of China (No. 51379160). H. B. acknowledges the support from the National Natural Science Foundation of China (No. 51306111) and the Shanghai Municipal Natural Science Foundation (No. 13ZR1456000). Y. Y. is grateful for the support from the National Natural Science Foundation of China (No. 51206124 and 51428603). Y. Y. appreciates the discussion with Prof. Nuo Yang from Huazhong University of Science and Technology.

References

1 K. Takeda and K. Shiraishi, *Phys. Rev. B: Condens. Matter Mater. Phys.*, 1994, **50**, 14916.
2 M. Hu, X. Zhang and D. Poulikakos, *Phys. Rev. B: Condens. Matter Mater. Phys.*, 2013, **87**, 195417.
3 A. Kara, H. Enriquez, A. P. Seitsonen, L. C. Lew Yan Voon, S. Vizzini, B. Aufray and H. Oughaddou, *Surf. Sci. Rep.*, 2012, **67**, 1.
4 B. Lalmi, H. Oughaddou, H. Enriquez, A. Kara, S. Vizzini, B. Ealet and B. Aufray, *Appl. Phys. Lett.*, 2010, **97**, 223109.
5 H. P. Li and R. Q. Zhang, *EPL*, 2012, **99**, 36001.
6 T. Ng, J. Yeo and Z. Liu, *Int. J. Mech. Mater. Des.*, 2013, **9**, 105.
7 Q.-X. Pei, Y.-W. Zhang, Z.-D. Sha and V. B. Shenoy, *J. Appl. Phys.*, 2013, **114**, 033526.
8 B. Liu, C. D. Reddy, J. W. Jiang, H. W. Zhu, J. A. Baimova, S. V. Dmitriev and K. Zhou, *J. Phys. D: Appl. Phys.*, 2014, **47**, 165301.
9 X. Gu and R. Yang, *J. Appl. Phys.*, 2015, **117**, 025102.
10 H. Xie, M. Hu and H. Bao, *Appl. Phys. Lett.*, 2014, **104**, 131906.
11 X. Zhang, H. Xie, M. Hu, H. Bao, S. Yue, G. Qin and G. Su, *Phys. Rev. B: Condens. Matter Mater. Phys.*, 2014, **89**, 054310.
12 J. Tersoff, *Phys. Rev. B: Condens. Matter Mater. Phys.*, 1988, **37**, 6991.
13 Z. Wang, T. Feng and X. Ruan, *J. Appl. Phys.*, 2015, **117**, 084317.
14 S. Cahangirov, M. Topsakal, E. Aktürk, H. Şahin and S. Ciraci, *Phys. Rev. Lett.*, 2009, **102**, 236804.
15 J. C. Garcia, D. B. de Lima, L. V. C. Assali and J. F. Justo, *J. Phys. Chem. C*, 2011, **115**, 13242.
16 D. Kaltsas, L. Tsetseris and A. Dimoulas, *Appl. Surf. Sci.*, 2014, **291**, 93.
17 T. Kumagai, S. Izumi, S. Hara and S. Sakai, *Comput. Mater. Sci.*, 2007, **39**, 457.
18 M. I. Baskes, *Phys. Rev. B: Condens. Matter Mater. Phys.*, 1992, **46**, 2727.
19 L. Bo, C. D. Reddy, J. Jinwu, Z. Hongwei, A. B. Julia, V. D. Sergey and Z. Kun, *J. Phys. D: Appl. Phys.*, 2014, **47**, 165301.
20 F. H. Stillinger and T. A. Weber, *Phys. Rev. B: Condens. Matter Mater. Phys.*, 1985, **31**, 5262.
21 S. Plimpton, *J. Comput. Phys.*, 1995, **117**, 1.
22 S. Munetoh, T. Motooka, K. Moriguchi and A. Shintani, *Comput. Mater. Sci.*, 2007, **39**, 334.
23 A. K. Rappe, C. J. Casewit, K. S. Colwell, W. A. Goddard and W. M. Skiff, *J. Am. Chem. Soc.*, 1992, **114**, 10024.
24 C. L. Lin, R. Arafune, K. Kawahara, N. Tsukahara, E. Minamitani, Y. Kim, N. Takagi and M. Kawai, *Appl. Phys. Express*, 2012, **5**, 045802.
25 P. Vogt, P. De Padova, C. Quaresima, J. Avila, E. Frantzeskakis, M. C. Asensio, A. Resta, B. Ealet and G. Le Lay, *Phys. Rev. Lett.*, 2012, **108**, 155501.
26 Q. Wang, C. Wang, Y. Zhang and T. Li, *Nucl. Instrum. Methods Phys. Res., Sect. B*, 2014, **328**, 42.
27 S. S. Mahajan, G. Subbarayan and B. G. Sammakia, *IEEE Intersoc. Conf. Therm. Thermomech. Phenom. Electron. Syst., 12th*, 2008, 1055.
28 J. C. Zhang and X. W. Wang, *Nanoscale*, 2013, **5**, 734.
29 B. Liu, J. A. Baimova, C. D. Reddy, S. V. Dmitriev, W. K. Law, X. Q. Feng and K. Zhou, *Carbon*, 2014, **79**, 236.
30 Q. Y. Wang, C. L. Wang, Y. Zhang and T. S. Li, *Nucl. Instrum. Methods Phys. Res., Sect. B*, 2014, **328**, 42.

31 Y. Ni, Y. Chalopin and S. Volz, 6th European Thermal Sciences Conference (Eurotherm 2012), 2012, p. 395.
32 S. Merabia and K. Termentzidis, *Phys. Rev. B: Condens. Matter Mater. Phys.*, 2012, **86**, 094303.
33 S. S. Mahajan, G. Subbarayan and B. G. Sammakia, *2008 11th IEEE Intersociety Conference on Thermal and Thermomechanical Phenomena in Electronic Systems*, 2008, vol. 1–3, p. 1055.
34 V. Samvedi and V. Tomar, *Nanotechnology*, 2009, **20**, 365701.
35 B. Liu, J. A. Baimova, C. D. Reddy, A. W. K. Law, S. V. Dmitriev, H. Wu and K. Zhou, *ACS Appl. Mater. Interfaces*, 2014, **6**, 18180.
36 J. Zhang, Y. Hong and Y. Yue, *J. Appl. Phys.*, 2015, **117**, 134307.
37 B. Liu, F. Meng, C. D. Reddy, J. A. Baimova, N. Srikanth, S. V. Dmitriev and K. Zhou, *RSC Adv.*, 2015, **5**, 29193.
38 J. Zhang, Y. Wang and X. Wang, *Nanoscale*, 2013, **5**, 11598.
39 Y. Hong, L. Li, X. C. Zeng and J. Zhang, *Nanoscale*, 2015, **7**, 6286.
40 L. Chen, Z. Huang and S. Kumar, *Appl. Phys. Lett.*, 2013, **103**, 123110.
41 Z.-Y. Ong and E. Pop, *Phys. Rev. B: Condens. Matter Mater. Phys.*, 2010, **81**, 155408.
42 B. Liu, J. A. Baimova, C. D. Reddy, A. W.-K. Law, S. V. Dmitriev, H. Wu and K. Zhou, *ACS Appl. Mater. Interfaces*, 2014, **6**, 18180.
43 H. P. Li and R. Q. Zhang, *EPL*, 2014, **105**, 56003.
44 Y. Zhang, J. X. Cao, Y. Xiao and X. H. Yan, *J. Appl. Phys.*, 2007, **102**, 104303.
45 M. Li, J. Zhang, X. Hu and Y. Yue, *Appl. Phys. A: Mater. Sci. Process.*, 2015, **119**, 415.
46 H. Wada and T. Kamijoh, *Jpn. J. Appl. Phys., Part 2*, 1996, **35**, L648.
47 Y. Yue, J. Zhang, X. Tang, S. Xu and X. Wang, *Nanotechnol. Rev.*, 2015, DOI: 10.1515/ntrev-2014-0024.
48 J. Zhang, X. Wang and H. Xie, *Phys. Lett. A*, 2013, **377**, 721.
49 J. Zhang, X. Wang and H. Xie, *Phys. Lett. A*, 2013, **377**, 2970.
50 X. Zhang, H. Bao and M. Hu, *Nanoscale*, 2015, **7**, 6014.
51 K.-X. Chen, X.-M. Wang, D.-C. Mo and S.-S. Lyu, *Chem. Phys. Lett.*, 2015, **618**, 231.
52 Z.-X. Guo, J. W. Ding and X.-G. Gong, *Phys. Rev. B: Condens. Matter Mater. Phys.*, 2012, **85**, 235429.
53 E. Pop, V. Varshney and A. K. Roy, *MRS Bull.*, 2012, **37**, 1273.

 This journal is © the Owner Societies 2015